The Aeronautical Journal (2025), **129**, pp. 1750–1763
doi:10.1017/aer.2024.156

RESEARCH ARTICLE

Integration of CFO-based three-dimensional target manoeuver compensation guidance rate and transition region optimisation algorithm

G.Y. Qi[1], X.L. Zhang[1], L.Y. Li[1,2], S.S. Wang[1] and H.Y. Zhang[3]

[1]School of Control Science and Engineering, Tiangong University, Tianjin, China
[2]Key Laboratory of UAV Emergency Rescue Technology, Ministry of Emergency Management, China
[3]The National Research Base of Intelligent Manufacturing Service, Chongqing Technology and Business University, Chongqing, China
Corresponding author: L.Y. Li; Email: liliya@tiangong.edu.cn

Received: 25 September 2024; **Revised:** 13 November 2024; **Accepted:** 4 December 2024

Keywords: terminal guidance; mid-course and terminal handover; maneuver compensation control; interceptor

Abstract

To address the challenges of high-manoeuver targets and limited line-of-sight from the interceptor's side window, this paper proposes a three-dimensional target manoeuver compensation control (TMCC) guidance law based on compensation function observe (CFO) and a method for studying the terminal guidance handover region. First, a relative model of the missile-target engagement is established. Secondly, the CFO is used to estimate the target manoeuver state, and the estimated information is fed back to the controller of the orbit control engine to make the interception more accurate. Considering the limited line of sight of the side window, the body line of sight angle is constrained by controlling the attitude control engine. Then, the problem description for solving the handover area and the definition of the terminal guidance handover area were provided, and the algorithm design for the handover area was conducted, simplifying the solving process through the concept of area substitution. Simulation results indicate that the proposed terminal guidance law offers higher interception accuracy compared to traditional proportional guidance, and effectively validates the accuracy of the handover region calculation.

Nomenclature

M	interceptor
T	intercept target
R	relative distance
$V_{M,sap}$, $V_{T,sap}$	the velocity of longitudinal plane interceptor and target, respectively
$a_{M,sap}$, $a_{T,sap}$	the acceleration of longitudinal plane interceptor and target, respectively
F_g	thrust of orbit control engine
$a_{M,tap}$, $a_{T,tap}$	the acceleration of transverse plane interceptor and target, respectively
k_{1q}	line of sight angle controller parameter
e_1	the line-of-sight tracking error
F_{tg}	rail controlled engine thrust
l_1, l_2	observer CFO coefficients
z_1, z_2, z_3	observer CFO status variables
S_T	target area
T_c	terminal guidance time
P_{T_0}	centre point of target area

© The Author(s), 2025. Published by Cambridge University Press on behalf of Royal Aeronautical Society.

https://doi.org/10.1017/aer.2024.156 Published online by Cambridge University Press

Greek symbol

q_θ	the line-of-sight angle of the longitudinal plane
θ_M, θ_T	the ballistic inclination of interceptor and target, respectively
ϑ	interceptor pitch angle
$q_{\theta b}$	interceptor stereoline angle
ψ_M, ψ_T	the horizontal plane interceptor and the target
q_ψ	the line-of-sight angle of the longitudinal plane
ψ	definition text definition text
ω_z	interceptor pitch angular velocity
q_{θ_r}	expected line-of-sight angle
$\ddot{q}_{\theta r}$	expected line-of-sight angular acceleration

1.0 Introduction

Kinetic energy interceptor has the advantages of high lethality, small size and high speed, and has become an important measure of extra atmospheric missile defense [1]. In recent years, the terminal guidance method for manoeuvering targets, with miss distance as the core, has high research value [2]. Among them, proportional navigation has the characteristics of simple. efficient and practical [3–5], and has been widely promoted. However, the traditional proportional navigation [6] still has shortcomings in the face of high manoeuvering targets.

At present, there are many researches on terminal guidance interception methods, especially the optimal guidance law is widely used [7–10]; The three-dimensional guidance law proposed by Kumar et al. [11] used coupling dynamics to reduce the control workload; Hu et al. [12] proposed a three-dimensional twisting control guidance law, which employs a robust adaptive multivariable twisting control method to simultaneously drive the line-of-sight angle and rate tracking errors to a predetermined zero neighbourhood in two orthogonal planes; references(13–16) proposed a cooperative guidance law, which can intercept the same target by multiple missiles; Sun et al. [17] added an extended state observer to the guidance law, which effectively shortened the interception time; Du et al. [18] proposed a flight estimation method, which can calculate the missile hit time; Zheng et al. [19] proposed a guiding law that overcomes the issues of large initial control inputs and oscillations in existing sliding mode guidance; Han et al. [20,21] proposed the terminal angle constraint incremental guidance method suitable for tactical missiles; there are also many improvements on the original proportional guidance. Cho et al. [22] incorporated impact time control into proportional guidance, overcoming issues such as narrow capture regions, limited initial conditions, and constrained impact times; Chen et al. [23] proposed a cooperative guidance law based on proportional guidance to avoid singularity when the guidance angle is close to zero; Zhang et al. [24] proposed a new impact angle control guidance law against a stationary target in the three-dimensional (3D) plane; Wang et al. [25] added terminal acceleration constraints to proportional guidance, enabling interception of the target at the desired attack angle even under line-of-sight angle limitations; Su et al. [26] proposed a new close-range biased proportional guidance rate, which consumes less fuel compared to the traditional proportional guidance; Wu et al. [27] designed the actor-critic networks and corresponding adaptive weight update laws to cope with unknown disturbances, but this method is more complex than using an observer to estimate disturbances, making guidance more difficult; Prasanna et al. [28] introduced a new proportional navigation guidance law, which offers a larger capture region compared to the classical proportional guidance. These documents are all improvements on the original guidance law and do not use real-time fusion compensation of estimation information to the guidance law. Therefore, designing a terminal guidance method for interceptors targeting highly manoeuverable targets with limited measurement capabilities is a key issue that this paper seeks to address, in order to achieve precise interception of manoeuvering targets in complex scenarios without relying on complex guidance parameter design and calculations. The innovation and contribution of this paper are as follows:

https://doi.org/10.1017/aer.2024.156 Published online by Cambridge University Press

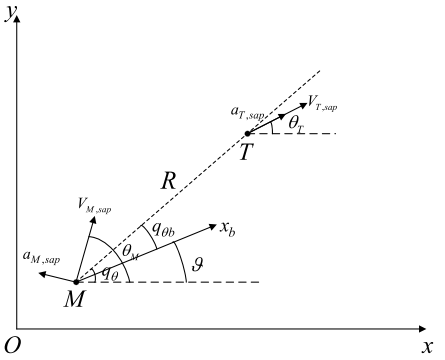


Figure 1. *Relative position of longitudinal plane.*

(1) Literatures mentioned above mostly focus on incorporating terminal angle and end acceleration constraints into the guidance laws, emphasising improvements under energy constraints. However, they fall short in intercepting highly manoeuverable targets. This paper introduces an observer-based CFO to estimate the target's manoeuvering state and integrates this state information into the guidance law. Compared to traditional proportional guidance, this guidance law significantly enhances the tracking capability for highly manoeuverable targets and reduces interception time. Additionally, it demonstrates greater robustness against target manoeuvering changes and external disturbances, thereby improving interception accuracy.

(2) Due to the short duration of the terminal guidance phase and the strong manoeuverability of the target, improper handover between midcourse and terminal guidance makes interception difficult. To address this issue, this paper proposes a calculation method for the midcourse-to-terminal handover zone. Performing terminal guidance within the calculated handover zone can effectively engage the target.

2.0 Missile target relative model

The interceptor is controlled by attitude and trajectory control engines as input, and the attitude and orbit control engines are installed perpendicular to the longitudinal axis of the projectile. The trajectory control engine is installed at the interceptor centroid to provide force control quantity and adjust its flight trajectory by changing acceleration; The attitude control engine is installed at the rear of the interceptor and both force and torque control are provided. The torque control is primarily used for attitude correction. By controlling the orbit control engine to strike the target accurately, and controlling the attitude control engine to make the seeker side window observe the target.

Taking the longitudinal plane as an example, the geometric relationship between the relative motion of the interceptor and the target is shown in Fig. 1. M stands for interceptors; T is intercept target; R represents relative distance; q_θ is the line of sight angle of the longitudinal plane, $V_{M,sap}$, $V_{T,sap}$ represent the velocity of longitudinal plane interceptor and target, respectively, θ_M, θ_T represent the ballistic inclination of interceptor and target, respectively, x_b coincides with the interceptor longitudinal axis and points to the interceptor head; ϑ is interceptor pitch angle and $q_{\theta b}$ stands for interceptor stereoline angle.

According to the relative geometric relationship between the interceptor target and target in Fig. 1, the kinematic model of the near space kinetic energy interceptor in the longitudinal plane can be established as

https://doi.org/10.1017/aer.2024.156 Published online by Cambridge University Press

$$\begin{aligned}\dot{R} &= V_{T,sap}\cos(q_\theta - \theta_T) - V_{M,sap}\cos(q_\theta - \theta_M)\\ R\dot{q}_\theta &= V_{M,sap}\sin(q_\theta - \theta_M) - V_{T,sap}\sin(q_\theta - \theta_T)\\ \dot{\theta}_{M,sap} &= \frac{a_{M,sap}}{V_{M,sap}}\end{aligned} \tag{1}$$

therefore

$$\ddot{q}_\theta = -\frac{2\dot{R}}{R}\dot{q}_\theta - \frac{a_{M,sap}\cos(q_\theta - \theta_M)}{R} - \frac{a_{T,sap}\sin(q_\theta - \theta_T)}{R} \tag{2}$$

where $a_{M,sap} = \frac{F_g}{m}$, F_g represents thrust of orbit control engine, m is interceptor mass and $a_{T,sap}$ is estimated by CFO and is fed back to the controller. Similarly, the transverse plane motion model can be obtained as

$$\ddot{q}_\psi = -\frac{2\dot{R}}{R}\dot{q}_\psi - \frac{a_{M,tap}\cos\left(q_\psi - \psi_M\right)}{R} - \frac{a_{T,tap}\sin\left(q_\psi - \psi_T\right)}{R} \tag{3}$$

where $a_{M,tap}$, $a_{T,tap}$ represent the acceleration of the transverse plane interceptor and the target, respectively, ψ_M, ψ_T respectively, stand for the ballistic deflection angle between the horizontal plane interceptor and the target; q_ψ is the line of sight angle of the longitudinal plane.

Since the kinetic energy interceptor adopts the full strapdown seeker, the relationship between the stereoscopic line angle of the kinetic energy interceptor and the azimuth angle of the target line and the elevation angle of the interceptor is as follows

$$q_{\theta b} = q_\theta - \vartheta \tag{4}$$

where $\dot{\vartheta} = \omega_z$.

Considering the field of view limitation of the full strapdown seeker, $q_{\theta b}$ needs to satisfy the following constraints

$$\varepsilon_{\min} < q_{\theta b} < \varepsilon_{\max} \tag{5}$$

where $\varepsilon_{\min}$ and $\varepsilon_{\max}$ represent the maximum and minimum field of view angles of the seeker, respectively, both of which are constants.

3.0 Design and stability analysis of the target manoeuver compensation guidance law

This chapter is divided into two sections. The first section covers the design of a three-dimensional guidance law for target manoeuver compensation. It begins by presenting the missile-target relative model and deriving the control rate for the trajectory control engine. Due to limitations on the seeker's line-of-sight angle, a pitch channel model for the interceptor missile is developed to design the control rate for the attitude control engine. The second section applies the Hurwitz stability criterion to verify the stability of the proposed guidance law.

3.1 Guiding principle design

For example, in the longitudinal plane, it can be simplified as

$$\ddot{q}_\theta = f_0 + f_d + b_1 u_1 \tag{6}$$

where $f_0 = -\frac{2\dot{R}}{R}\dot{q}_\theta - \frac{a_{T_0}\sin(q_\theta - \theta_T)}{R}$, $f_d = -\frac{a_{Td}\sin(q_\theta - \theta_T)}{R}$, $b_1 = -\frac{F_{tg}\cos(q_\theta - \theta_M)}{mR}$, $u_1 = \tau_g$.

Assuming the desired line-of-sight angle is $q_{\theta r}$, set the tracking error as $e_{1q} = q_{\theta r} - q_\theta$. The tracking error equation is

$$\dot{e}_{1q} = -k_{1q}e_{1q} + \left(k_{1q}e_{1q} + \ddot{q}_{\theta r} - (f_0 + f_d + b_1 u_1)\right) \tag{7}$$

https://doi.org/10.1017/aer.2024.156 Published online by Cambridge University Press

let ${}_{1q}e_{1q} + \ddot{q}_{\theta r} - (f_0 + f_d + b_1 u_1) = 0$. Thus, the nonlinear controller that ensures the exponential asymptotic stability of the closed-loop system is given by

$$u_1 = \frac{1}{b_1}\left(k_{1q}e_{1q} + \ddot{q}_{\theta r} + \frac{2\dot{R}}{R}\dot{q}_\theta + \frac{a_{T_0}\sin(q_\theta - \theta_T)}{R} + f_d\right) \tag{8}$$

where f_d can be obtained from the CFO designed by Qi et al. [29]. k_{1q} can be determined through pole placement. $\ddot{q}_{\theta r}$ can be extracted from the HOD in Ref. [30].

The pitch channel model of the interceptor can be simplified to

$$\ddot{\vartheta} = f_d + b_2 u_2 \tag{9}$$

where f_d represents unknown disturbances and unmodeled components, $b_2 = -\frac{1}{J_z}F_{tz}L$, $u_2 = \tau_z$. Define the tracking error as $e_{1\vartheta} = \vartheta_r - \vartheta$ and $e_{2\vartheta} = \dot{\vartheta}_r - \dot{\vartheta}$. Thus, the tracking error is

$$\begin{cases} \dot{e}_{1\vartheta} = e_{2\vartheta} \\ \dot{e}_{2\vartheta} = -k_{2\vartheta}e_{1\vartheta} - k_{1\vartheta}e_{2\vartheta} + \left(k_{2\vartheta}e_{1\vartheta} + k_{1\vartheta}e_{2\vartheta} + \ddot{\vartheta}_r - (f_d + b_2 u_2)\right) \end{cases} \tag{10}$$

let $k_{2\vartheta}e_{1\vartheta} + k_{1\vartheta}e_{2\vartheta} + \ddot{q}_{\theta r} - (f_d + b_2 u_2) = 0$, the nonlinear controller that ensures the closed-loop system is exponentially asymptotically stable is defined as

$$u_2 = \frac{1}{b_2}\left(k_{2\vartheta}e_{1\vartheta} + k_{1\vartheta}e_{2\vartheta} + \ddot{\vartheta}_r - f_d\right) \tag{11}$$

3.2 Guiding law stability analysis

Theorem 1. *For missile target relative model (6), the trajectory control engine controller (8) is used to control the line-of-sight angle. When the controller gain $k_{1q} > 0$, the characteristic polynomial is Hurwitz polynomial, the system is asymptotically stable, and the Los tracking error converges asymptotically.*

Lemma 1. *Qi et al. [29] demonstrated in their study that the CFO exhibits exponential stability under the condition of $\lambda l_1^2 + l_1 l_2 - l_2 > 0$. Assuming f is a third-order infinitesimal, then $\lim_{t\to\infty}\hat{f} = f_d$.*

The third-order CFO model is

$$\begin{aligned} \dot{z}_1 &= z_2 \\ \dot{z}_2 &= Le + z_3 + bu \\ \dot{z}_3 &= \lambda Le \\ \hat{f} &= Le + z_3 \end{aligned} \tag{12}$$

where $L = \begin{bmatrix} l_2 & l_1 \end{bmatrix}$, $e = \begin{bmatrix} e_1 & e_2 \end{bmatrix}^T$. According to Lemma 1, the Equation (12) is asymptotically stable under the condition $\lambda l_1^2 + l_1 l_2 - \lambda l_2 > 0$. Under the assumption that f is a third-order infinitesimal, the observed state $\hat{f}$ converges to the unknown function f_d, and the steady-state error is zero.

Proof. The missile-target relative model is given by

$$\ddot{q}_\theta = -\frac{2\dot{R}}{R}\dot{q}_\theta - \frac{a_{T_0}\sin(q_\theta - \theta_T)}{R} - f_d - \frac{F_{tg}\cos(q_\theta - \theta_M)}{mR}\tau_g \tag{13}$$

Define the tracking error as $e_1 = q_{\theta r} - q_\theta$, From Equation (13), the tracking error equation is

$$\dot{e}_1 = -k_{1q}e_{1q} + \left(k_{1q}e_{1q} + \ddot{q}_{\theta r} + \frac{2\dot{R}}{R}\dot{q}_\theta + \frac{a_{T_0}\sin(q_\theta - \theta_T)}{R} + f_d + \frac{F_{tg}\cos(q_\theta - \theta_M)}{mR}\tau_g\right) \tag{14}$$

https://doi.org/10.1017/aer.2024.156 Published online by Cambridge University Press

Let ${}_{1q}e_{1q} + \ddot{q}_{\theta r} + \frac{2\dot{R}}{R}\dot{q}_{\theta} + \frac{a_{T_0}\sin(q_{\theta}-\theta_T)}{R} + f_d + \frac{F_{tg}\cos(q_{\theta}-\theta_M)}{mR}\tau_g = 0$, the available line of sight angle controller is

$$\tau_g = -\frac{mR}{F_{tg}\cos(q_{\theta}-\theta_M)}\left(k_{1q}e_{1q} + \ddot{q}_{\theta r} + \frac{2\dot{R}}{R}\dot{q}_{\theta} + \frac{a_{T_0}\sin(q_{\theta}-\theta_T)}{R} + f_d\right) \tag{15}$$

then the tracking error equation becomes

$$\dot{e}_1 = -k_{1q}e_{1q} \tag{16}$$

When $k_{1q} > 0$, it can be seen from the Hurwitz criterion that the parameter polynomial qualifies as a Hurwitz polynomial, indicating that the system is stable.

$$\lim_{t\to\infty} q_{\theta} = q_{\theta r} \tag{17}$$

Therefore, the interceptor line of sight angle q_{θ} converges to the desired angle $q_{\theta r}$ with zero steady-state error.

The proof is completed.

4.0 Terminal guidance handover region

Missile interception is divided into two phases: the midcourse guidance phase and the terminal guidance phase. The handover region is the area where the missile transitions from midcourse guidance to terminal guidance. Due to the uncertainties in target manoeuvering during the terminal guidance phase and various environmental interferences, the actual trajectory of the target often deviates from the predicted trajectory. This deviation can result in the target's final position being located within a region known as the target area. Therefore, it is necessary to identify a location within this region for terminal guidance so that the interceptor missile can engage all possible positions within the target area. In this paper, the set of positions from which the missile can effectively engage all locations within the target area is referred to as the terminal guidance handover region.

4.1 Problem description

(1) Target area
The target area is defined as the region consisting of all possible positions of the target after a certain time, taking into account target manoeuverability and environmental effects. Due to the uncertainty in defining this area, a circular approximation is used in this paper, though the method is applicable to target areas of any shape.

(2) Handover region
The handover region is defined as the area consisting of all points within the space that can be reached under certain time and speed constraints. In other words, this is the region where the interceptor missile transitions to terminal guidance, ensuring that the missile is capable of hitting the enemy missile within the target area during the terminal guidance phase.

Define the target area as S_T, the initial speed of the missile during the terminal guidance phase is v_0, axial average speed is

$$v_{\perp} = \bar{V}n\,,\ n = \left(I - \frac{v_0 v_0^T}{{v_0}^2}\right)\frac{x}{x}\,,\ x \in R^3 \tag{18}$$

where $v_{\perp}$ is the axial average speed. If the missile's axial speed eventually accelerates to $V_{\max}$, the magnitude of the average speed is $\bar{V}$, and n is a unit vector perpendicular to the initial speed v_0.

Considering the missile as a point mass, the motion model can be represented as

$$\dot{p} = v \tag{19}$$

https://doi.org/10.1017/aer.2024.156 Published online by Cambridge University Press

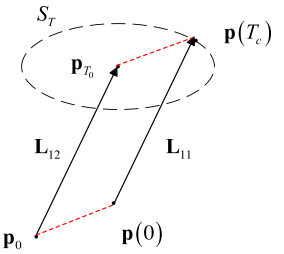


Figure 2. *Vector substitution.*

where p is the missile's position and v is the missile's velocity. Assume the terminal guidance time is T_c. If the target is hit, then $p\,(T_c) \in S_T$. Find the set of $p\,(0)$ for which

$$p\,(T) = p\,(0) + \int_0^{T_c} v\,(s)\,ds \tag{20}$$

therefore

$$\begin{aligned} p\,(0) &= p\,(T_c) - \int_0^{T_c} v\,(s)\,ds \\ &= p\,(T_c) - v_0 T_c - \bar{V}\left(I - \frac{v_0 v_0^T}{{v_0}^2}\right)\frac{x}{x} T_c \end{aligned} \tag{21}$$

Solution of the handover region:

Give v_0 and $\forall p_T \in S_T$, investigate the existence of $0 \le T_c \le T_{\max}$ where a missile starting from $p\,(0)$ will satisfy $p\,(T_c) = p_T$ at time T_c. The set of such $p\,(0)$ forms a region called the handover region.

4.2 Design concept

In investigating the transition region, it is necessary to determine every transition point $p\,(0)$ in space and verify whether $p\,(0)$ can reach all positions within the target region S_T. Due to variations in these initial values, this leads to significant redundant calculations. This paper transforms the problem and explores a solution method that significantly reduces the computational load.

Take a point $p_{T_0} \in S_T$ (often the centre point) in S_T, the starting point is $p\,(0)$, and the vector from $\forall p\,(T) \in S_T$, $p\,(0)$ to $p\,(T_c)$ is called $L_{11} = p\,(T_c) - p\,(0)$. There is a point p_0 in space, and the vector from p_0 to p_{T_0} is $L_{12} = p_{T_0} - p_0$, so that $L_{11} = L_{12}$, then

$$\begin{aligned} & p_0 - p\,(0) \\ &= p_0 - p_{T_0} + p_{T_0} - p\,(T_c) + p\,(T_c) - p\,(0) \\ &= p\,(0) - p\,(T_c) + p_{T_0} - p\,(T_c) - p\,(0) \\ &= p_{T_0} - p\,(T_c) \end{aligned} \tag{22}$$

That is, the vector from p_0 to $p\,(0)$ is equal to the vector from p_{T_0} to $p\,(T_c)$, as shown in Fig. 2.

Similarly, the vector L_{n1} of $\forall p\,(T) \in S_T$ and $p\,(0)$ corresponds to the vector L_{n2} of p_0 and p_{T_0}, and the region S_T centred on p_{T_0} also corresponds to the region S_M centred on $p\,(0)$. As shown in Fig. 3.

Figure 3 shows the initial conversion of the solution target, which explores whether a specific point can reach all positions within the target area. It involves transforming all points in a spatial area with the same shape as the target area to converge at the centre of the target area, where the centre point serves as the feasible point for shift handover.

Given v_0, $\forall p_0 \in S_M$, calculate the T_c time from p_0 so that $p\,(T_c) = p_{T_0}$ under the conditions of $0 \le T_c \le T_{\max}$. Such p_0 is the feasible point for shift handover, and all p_0 constitute a set. Refer to Fig. 4 for details.

Set S_0 is the red area in Fig. 4, in which the centre of the target area can be reached. In the set S_0, we find that $S_M \subset S_0$ is satisfied, so the midpoint $p\,(0)$ of S_M can reach any area of the target. The central

https://doi.org/10.1017/aer.2024.156 Published online by Cambridge University Press

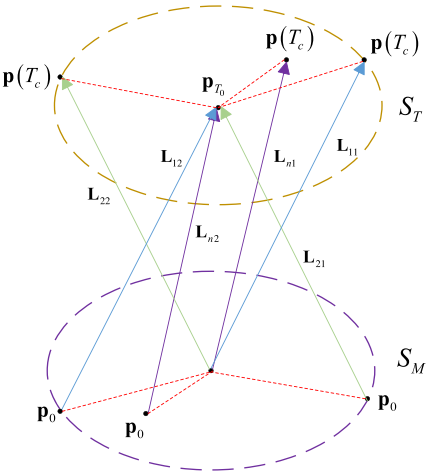


Figure 3. *Regional substitution.*

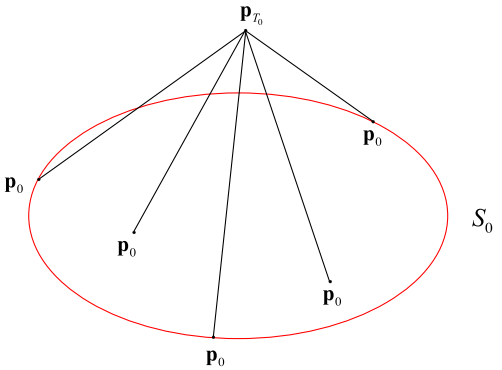


Figure 4. *Central area.*

point p (0) of these sets S_M forms a new set S_c, which is the feasible area of shift handover. As depicted in Fig. 5.

4.3 Design method

First, all positions in the solution space that can reach the centre of the target area are optimised. The optimisation objective is to minimise the position error at the intercept time. Constraints need to be added during the solution process, which can be expressed as follows:

$$\min_{a_m, t_h, T_c} \left\| p_0 + v_0 T_c + \frac{1}{2} a {T_c}^2 - p_{T_0} \right\|$$

$$s.t.$$

$$||a|| \leq 20\mathrm{m/s}^2$$

$$0s \leq T_c \leq 10\mathrm{s}$$

$$aT_c \cdot v_0 = 0 \tag{23}$$

where a is the missile's acceleration, T_c is the terminal guidance time, and p_{T_0} is the target area centre position.

https://doi.org/10.1017/aer.2024.156 Published online by Cambridge University Press

Table 1. *Target motion parameters*

Parameter	Value	Unit
Centre point of target area	$(16,500,\ 13,200,\ 11,000)$	m
Target area radius	200	m
Initial speed of terminal guidance	$(1,500,\ 1,200,\ 1,000)$	m/s

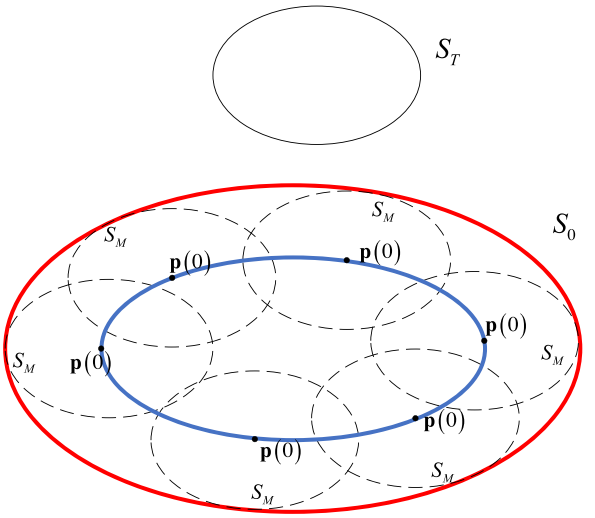


Figure 5. *Transition region.*

Then explore the placement of the target area within the region. Given the midpoint of the target area, judge whether the contour of the area is in the target area at the same time one by one. If it is true, the point is the handover point. The judgement method is as follows:

$$\Delta P_t = \begin{bmatrix} \Delta x_t \\ \Delta y_t \\ \Delta z_t \end{bmatrix}^T = r \begin{bmatrix} \sin\theta\ \sin\varphi \\ \sin\theta\ \cos\varphi \\ \cos\theta \end{bmatrix} \tag{24}$$

among them, the radius of the circle in the target area is r, the centre of the circle is $P_{t0} = \begin{bmatrix} x_{t0} & y_{t0} & z_{t0} \end{bmatrix}$, and the judgement position is $P_t = \Delta P_t + P_{t0}$. Changing θ , φ can change the P_t position, and uniformly sample θ , φ. If these sampling points are included in the interceptable set, it is considered that the shift handover area can intercept any target area point.

5.0 Simulation verification

First, the handover area of terminal guidance is calculated, and then the feasibility of the handover area is verified by the guidance law proposed in this paper. Table 1 shows the initial parameter settings for calculating the shift handover area.

The area from the space to the centre of the target presents a cone as a whole in Fig. 6, and the centre line of the cone is the ideal path without control. The closer the missile is to the target, the smaller the handover region becomes. This is due to the reduced terminal guidance time, which makes it more difficult for the missile to adjust its trajectory in time to strike the target.

After determining the transition region, simulation verification is performed using the guidance law proposed in this paper. Since the actual guidance model cannot strictly follow the planned path and is

https://doi.org/10.1017/aer.2024.156 Published online by Cambridge University Press

Table 2. *Verification of transition region parameter settings*

Parameter	Value	Unit
Missile position	(1, 500, 1, 200, 1, 000)	m
Initial velocity of missile	(1, 500, 1, 200, 1, 000)	m/s
Target position	(8, 500, 9, 200, 5, 000)	m
Target initial speed	(800, 400, 600)	m/s

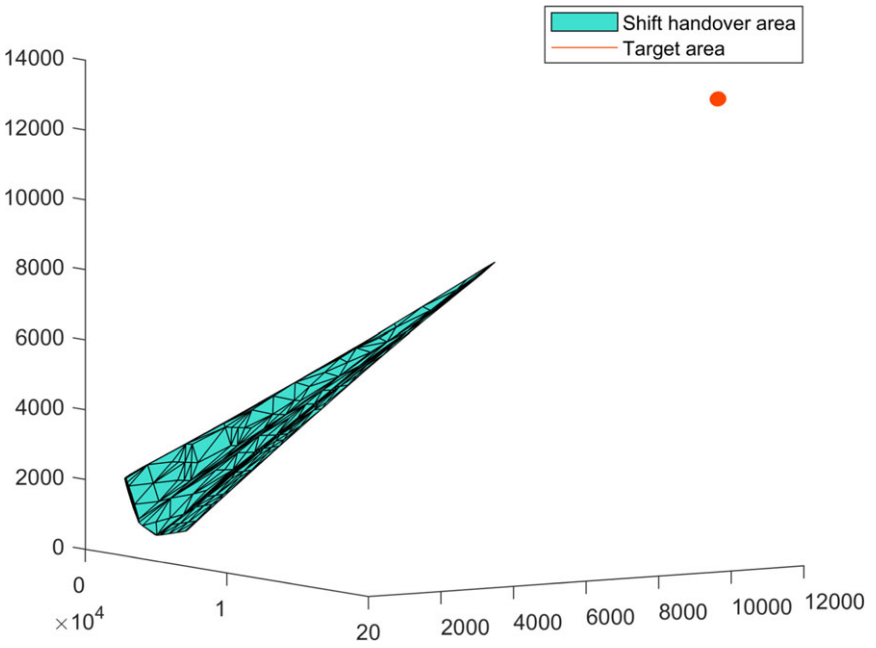


Figure 6. *Shift handover area calculation.*

affected by internal forces in the spatial environment, boundary points are avoided in the transition region during verification. Verification is completed by randomly selecting points in both the target region and the transition region. The initial parameter settings are shown in Table 2.

As shown in Fig. 7, arbitrary points selected from the calculated transition region and target region set can successfully complete the guidance control task. Although the missile acceleration was set as a constant value during planning, external force disturbances and the use of guidance laws instead of direct planning result in some deviation between the actual and planned paths. However, this does not affect its interceptability.

As depicted in Fig. 8(a), a comparison between the TMCC based on a compensator-observer and the traditional PN method indicates that TMCC has a shorter capture time and higher capture accuracy compared to the PN method. Figure 8(b) shows that a comparison between TMCC and PN trajectory control engine commands indicates that TMCC requires lower control input, thereby reducing energy consumption during the interception process. Use $\left|\int F_g \tau_g dt\right|$ to calculate the energy consumed.

It can be seen from Table 3 that TMCC has shorter intercept time and higher intercept accuracy than PN, because TMCC uses the acceleration information estimated by CFO to compensate the target acceleration into the controller, which uses more information than traditional PN and has higher accuracy. Compared with PN method, TMCC has smaller energy loss.

As there are certain requirements for the terminal guidance speed, there is a probability that interception may not be achievable. The following 6,000 groups are made to change the initial speed of the

https://doi.org/10.1017/aer.2024.156 Published online by Cambridge University Press

Table 3. *Interception results*

Method	Intercept time (s)	Interception accuracy(m)	Energy loss
Missile position	11.919	0.31	60,920
Initial velocity of missile	11.925	1.06	83,660

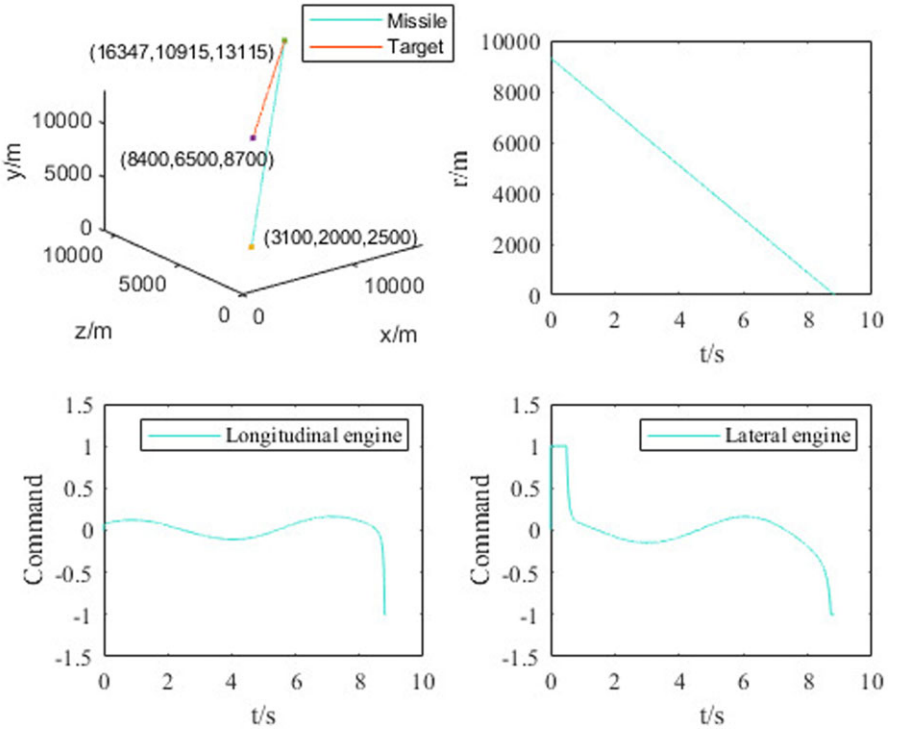


Figure 7. *Guidance simulation verification.*

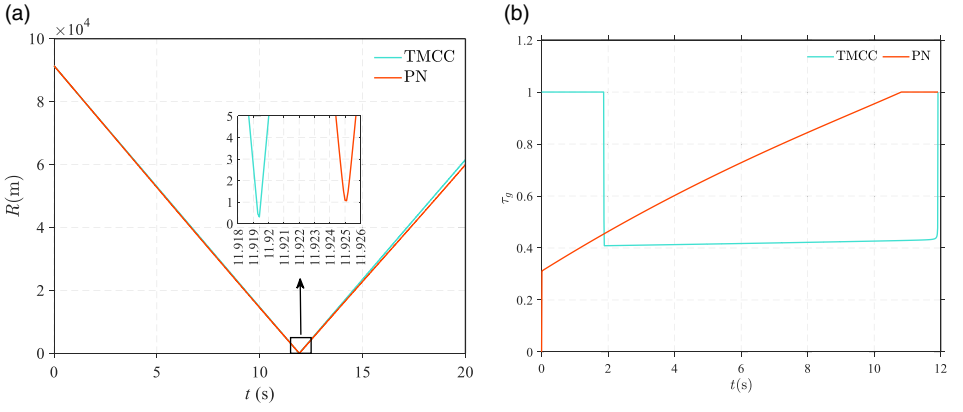


Figure 8. *Interception comparison chart.*

https://doi.org/10.1017/aer.2024.156 Published online by Cambridge University Press

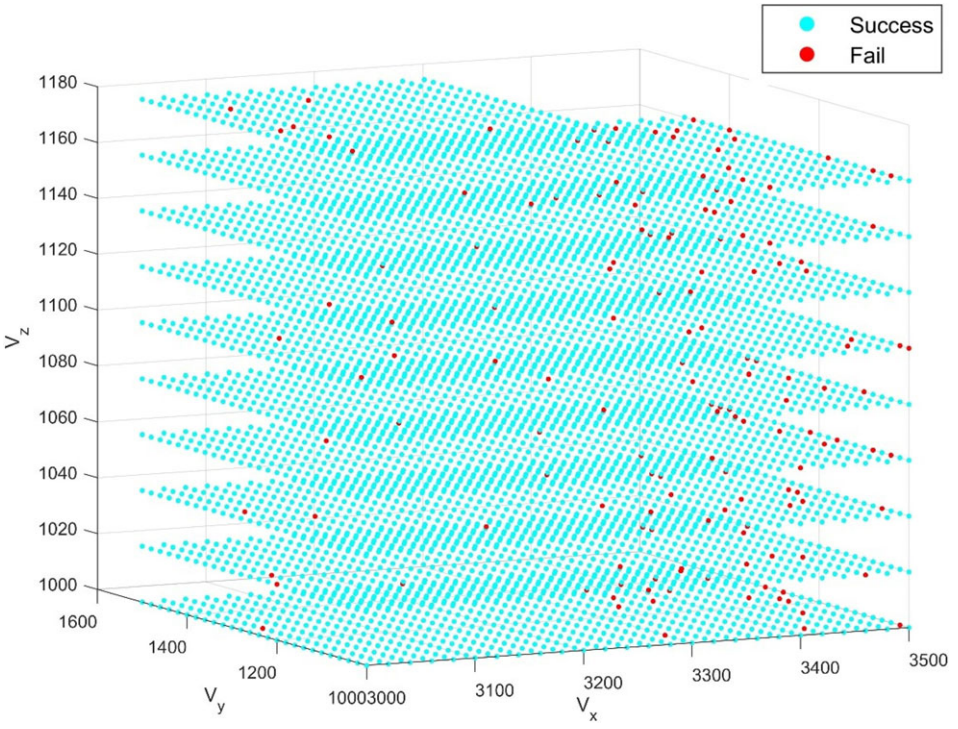


Figure 9. *Influence of interceptor initial velocity on interception.*

missile in the terminal guidance. Other parameter settings are the same as those in Table 2. If the miss distance is less than 1m, the interception will be considered successful, as shown in Fig. 9.

Figure 9 shows the initial speed of the missile in three directions and the interception. Blue represents the success of interception, and red represents the miss distance greater than 1m. It can be clearly seen that the success rate of interception is very high in the range of $1,000 \sim 1,600 m/s$ and $1,000 \sim 1,180 m/s$. The interception success rate is high at $3,000 \sim 3,200 m/s$, and the interception accuracy is a little lower when the speed exceeds 3,200m/s. Among the 6,000 groups of simulations, only 268 groups missed more than 1m. The guidance method designed in this paper has a high success rate in this scenario.

6.0 Conclusion

This paper presents a three-dimensional target manoeuver compensation guidance law based on CFO and a method for calculating the midcourse-to-terminal handover region. An observer-based CFO is employed to estimate the target's manoeuvering state and integrate this compensation into the guidance law. Additionally, a calculation method for the terminal guidance handover region is provided. When the target area is represented as a spherical shape, a conical-shaped handover region is derived. Finally, simulation validation is conducted in two parts. The first part involves simulating the midcourse-to-terminal handover region and validating it with the proposed guidance law, demonstrating that the computed handover region successfully completes the guidance control task. The second part compares the proposed guidance law with traditional proportional guidance. Due to the use of CFO to estimate the target's motion information and feed it back into the controller, the TMCC interception accuracy is higher and energy loss is lower compared to the PN method.

https://doi.org/10.1017/aer.2024.156 Published online by Cambridge University Press

Acknowledgements. This work was supported in part by the National Natural Science Foundation of China under Grant 62303350, the Natural Science Foundation of Tianjin City under Grant 23JCQNJC00660, Open Fund of Key Laboratory of UAV Emergency Rescue Technology, Ministry of Emergency Management (NO. UERT202402), China.

Competing interests. The authors declare that they have no known competing financial interests or personal relationships that could have appeared to influence the work reported in this paper.

References

[1] Chen, Y., Fang, Y.Z., Han, T. and Hu, Q.L. Incremental guidance method of kinetic energy interceptor based on target maneuver compensation, *J. Beijing Univ. Aeronaut. Astronaut.*, 2024, **50**, (3), pp 831–838.
[2] Yao, Y., Zheng, T.Y., He, F.H., Wang, L., Wang, Y., Zhang, X., Zhu, B.Y. and Yang, B.Q. Several hot issues and challenges in aircraft terminal guidance, *Acta Aeronaut. Astronaut. Sinica*, 2015, **8**, (3), pp 2696–2716.
[3] Adler, F.P. Missile guidance by three-dimensional proportional navigation, *J. Appl. Phys*, 1956, **27**, (5), pp 500–507.
[4] Jeon, I.S., Karpenko, M. and Lee, J.I. Connections between proportional navigation and terminal velocity maximization guidance, *J. Guid. Control Dyn.*, 2020, **43**, (2), pp 383–388.
[5] Paul, N. and Ghose, D. Qualitative analysis of variable speed proportional navigation guidance law, AIAA SCITECH, 2024, pp 1988.
[6] Ulybyshev Y. Terminal guidance law based on proportional navigation, *J. Guid. Control Dyn.*, 2005, **28**, (4), pp 821–824.
[7] Zhang, B.L. and Zhou, D. Optimal predictive sliding-mode guidance law for intercepting near-space hypersonic maneuvering target, *Chin. J. Aeronaut.*, 2022, **35**, (4), pp 320–331.
[8] Mian, G., Zhou, S.T. and Zhou, D. Optimal sliding mode guidance law against maneuvering target with impact angle constraint, *J. Aerospace Eng.*, 2024, **238**, (5), pp 513–528.
[9] Zhan, Y., Li, S. and Zhou, D. Time-to-go based three-dimensional multi-missile spatio-temporal cooperative guidance law: A novel approach for maneuvering target interception, *ISA Trans.*, 2024, **149**, pp 178–195.
[10] Luo, H.B., Tan, G.Y., Wang, X.H. and Ji, H.B. Cooperative line-of-sight guidance with optimal evasion strategy for three-body confrontation, *ISA Trans.*, 2023, **133**, pp 262–272.
[11] Kumar, S.R. and Ghose, D. Three-dimensional impact angle guidance with coupled engagement dynamics, *J. Aerospace Eng.*, 2017, **231**, (4), pp 621–641.
[12] Hu, Q.L., Han, T. and Xin, M. Three-dimensional guidance for various target motions with terminal angle constraints using twisting control, *IEEE Trans. Ind. Electron.*, 2019, **67**, (2), pp 1242–1253.
[13] Wang, X.H. and Lu, X. Three-dimensional impact angle constrained distributed guidance law design for cooperative attacks, *ISA Trans.*, 2018, **73**, pp 79–90.
[14] You, H., Chang, X.L., Zhao, J.F., Wang, S.H. and Zhang, Y.H. Three-dimensional impact-angle-constrained fixed-time cooperative guidance algorithm with adjustable impact time, *Aerospace Sci. Technol.*, 2023, **141**, pp 108574.
[15] Chen, Z.Y., Liu, X.M. and Chen, W.C. Three-dimensional event-triggered fixed-time cooperative guidance law against maneuvering target with the constraint of relative impact angles, *J. Franklin Inst.*, 2023, **360**, pp 3914–3966.
[16] Liu, S., Yan, B., Liu, R., Dai, P., Yan, J. and Xin, G. Cooperative guidance law for intercepting a hypersonic target with impact angle constraint, *Aeronaut. J.*, 2022, **1300**, pp 1026–1044.
[17] Sun, L.H., Wang, W.H., Yi, R. and Xiong, S.F. A novel guidance law using fast terminal sliding mode control with impact angle constraints, *ISA Trans.*, 2016, **64**, pp 12–23.
[18] Du, H., Yang, M., Wang, S. and Chao, T. Impact time guidance law for arbitrary lead angle using sliding mode control, *ISA Trans.*, 2024, **96**, (2), pp 307–315.
[19] Zheng, Z.W., Li, J.Z. and Feroskhan, M. Three-dimensional terminal angle constraint guidance law with class K∞ function-based adaptive sliding mode control, *Aerospace Sci. Technol.*, 2024, **147**, pp 109005.
[20] Han, T., Hu, Q.F., Shin, H.S., Tsourdos A. and Xin, M. Sensor-based robust incremental three-dimensional guidance law with terminal angle constraint, *J. Guid. Control Dyn.*, 2016, **44**, (11), pp 2016–2030.
[21] Han, T., Shin, H.S., Hu, Q.L., Tsourdos, A. and Xin, M. Differentiator-based incremental three-dimensional terminal angle guidance with enhanced robustness, *IEEE Trans. Aerospace Electron. Syst.*, 2022, **58**, (5) pp 4020–4032.
[22] Cho, N. and Kim, Y. Modified pure proportional navigation guidance law for impact time control, *J. Guid. Control Dyn.*, 2016, **39**, (4), pp 852–872.
[23] Chen, Y.D., Wang, J.N., Wang, C.Y., Shan, J.Y. and Xin, M. A modified cooperative proportional navigation guidance law, *J. Franklin Inst.*, 2019, **356**, (11), pp 5692–5705.
[24] Zhang, W.J. and Wang, B.M. A new guidance Law for impact angle constraints with time-varying navigation gain, *Aeronaut. J.*, 2022, **126**, (1304), pp 1752–1770.
[25] Wang, Y.N., Wang, H., Liu, D.F. and Wang, W. Nonlinear modified bias proportional navigation guidance law against maneuvering targets, *J. Franklin Inst.*, 2022, **359**, (7), pp 2949–2975.
[26] Su, W.S., Yao, D.N., Li, K.B. and Chen, L. A novel biased proportional navigation guidance law for close approach phase, *Chin. J. Aeronaut.*, 2016, **29**, (1), pp 228–237.
[27] Wu, T. and Wang, Z. Reinforcement learning-based adaptive spiral-diving manoeuver guidance method for reentry vehicles subject to unknown disturbances, *Aeronaut. J.*, 2024, **128**, (1328), pp 2218–2234.

https://doi.org/10.1017/aer.2024.156 Published online by Cambridge University Press

[28] Prasanna, H.M. and Ghose, D. Retro-proportional-navigation: a new guidance law for interception of high speed targets, *J. Guid. Control Dyn.*, 2012, **35**, (2), pp 377–386.
[29] Qi, G.Y., Li, X. and Chen, Z.Q. Problems of extended state observer and proposal of compensation function observer for unknown model and application in uav, *IEEE Trans. Syst. Man Cybern. Syst.*, 2021, **52**, (5), pp 2899–2910.
[30] Qi, G.Y., Chen, Z.Q. and Yuan, Z.Z. High order differential feedback control for nonlinear systems, *Eng. Sci.*, 2003, **5**, (8), pp 35–44.

Cite this article: Qi G.Y., Zhang X.L., Li L.Y., Wang S.S. and Zhang H.Y. (2025). Integration of CFO-based three-dimensional target manoeuver compensation guidance rate and transition region optimisation algorithm. *The Aeronautical Journal*, **129**, 1750–1763. https://doi.org/10.1017/aer.2024.156

https://doi.org/10.1017/aer.2024.156 Published online by Cambridge University Press